LAWRENCE
LIVERMORE
NATIONAL
LABORATORY

LLNL-CONF-654596

Modeling detachment physics in the NSTX snowflake divertor

E. T. Meier, V. A. Soukhanovskii, T. D. Rognlien, F. Scotti, R. E. Bell, A. Diallo, R. Kaita, B. P. LeBlanc, A. G. McLean, M. Podesta

May 19, 2014

21st International Conference on Plasma Surface Interactions 2014
Kanazawa, Japan
May 26, 2014 through May 30, 2014

Disclaimer

This document was prepared as an account of work sponsored by an agency of the United States government. Neither the United States government nor Lawrence Livermore National Security, LLC, nor any of their employees makes any warranty, expressed or implied, or assumes any legal liability or responsibility for the accuracy, completeness, or usefulness of any information, apparatus, product, or process disclosed, or represents that its use would not infringe privately owned rights. Reference herein to any specific commercial product, process, or service by trade name, trademark, manufacturer, or otherwise does not necessarily constitute or imply its endorsement, recommendation, or favoring by the United States government or Lawrence Livermore National Security, LLC. The views and opinions of authors expressed herein do not necessarily state or reflect those of the United States government or Lawrence Livermore National Security, LLC, and shall not be used for advertising or product endorsement purposes.

Modeling detachment physics in the NSTX snowflake divertor

E.T. Meier[a,*], V.A. Soukhanovskii[a], R.E. Bell[b], A. Diallo[b], R. Kaita[b], B.P. LeBlanc[b], A.G. McLean[a], M. Podesta[b], T.D. Rognlien[a], F. Scotti[a]

[a] *Lawrence Livermore National Laboratory, Livermore, California 94551, USA*
[b] *Princeton Plasma Physics Laboratory, Princeton, New Jersey 08540, USA*

Abstract

The snowflake divertor is a technique for coping with the tokamak power exhaust problem in next-step experiments and eventually reactors, where extreme power fluxes to material surfaces represent a leading technological and physics challenge. In lithium-conditioned National Spherical Torus Experiment (NSTX) discharges, application of the snowflake divertor typically induced partial detachment and severalfold heat flux reduction. UEDGEis used to analyze and compare conventional and snowflake divertor configurations in NSTX. Matching experimental upstream profiles and divertor diagnostics in the snowflake requires target recycling of 0.97 vs. 0.91 in the conventional case, implying partial saturation of the lithium-based pumping mechanism. Density scans are performed to analyze the mechanisms that facilitate detachment in the snowflake, revealing that increased divertor volume provides most of the parallel heat flux reduction, but neutral gas power loss, which is enhanced by the increased wetted area in the snowflake, plays a key role in enhancing volumetric recombination.

Keywords: snowflake, NSTX, divertor, fusion

1. Introduction

In ITER and other next-step magnetic fusion devices, power exhaust will threaten the integrity of divertor plasma-facing components [1]. In spherical tokamaks (STs), power exhaust is especially intense, due to a relatively small divertor footprint [2]. A variety of divertor heat flux mitigation research on the National Spherical Torus Experiment (NSTX) has aimed to build the physics understanding that will be critical to ITER operation, prepare for NSTX Upgrade [3] operation, and support divertor design for next-step STs [4]. Experiments with the snowflake divertor (SFD) configuration are the subject of the research presented here.

In the SFD [5], a secondary X-point is introduced near the primary X-point, providing heat flux mitigation through a variety of mechanisms [6]. In lithium-conditioned NSTX experiments, the SFD enabled partially detached divertor operation [7, 8] without the additional divertor deuterium injection required for such operation in conventional divertor configurations [9, 10]. Signatures of strong recombination were observed, including a dramatic increase in divertor D_α emission. Peak heat flux was typically reduced severalfold, from ~5 to ~1 MW/m^2.

The NSTX SFD experiments involve the intersection of two challenging areas of fusion physics research — divertor detachment and advanced divertor configuration — providing a particularly rich subject for modeling. The UEDGE code [11, 12], is used to analyze conventional divertor (CD) and SFD experimental results.

*Corresponding author
Email address: meier23@llnl.gov (E.T. Meier)

2. Modeling setup

UEDGE [11, 12] is a 2D multi-fluid edge transport code, based on the Braginskii two-fluid model [13]. Turbulent perpendicular transport is approximated with "effective" diffusivities. A fluid neutral model is employed. Two impurity models are available: one uses a fixed impurity concentration, and computes radiation assuming coronal conditions; the other is a charge-state-resolved model that tracks the density of individual impurity charge states. The research presented here focuses on results with a fixed fraction carbon model. Carbon concentration in the divertor region, where carbon radiation is most important, is unknown; 3% concentration, in rough agreement with upstream measurements, is chosen.

NSTX discharge 141240 is modeled at 439 and 905 ms, representing the CD and SFD phases, respectively. The LRDFIT Grad-Shafranov solver is used to generate equilibria at these times. Divertor regions of the UEDGE flux-fitted grids are presented in Fig. 1. Compared to the CD, the geometric expansion factor (accounting for both flux expansion and tilt of flux surfaces with respect to the target) for the SFD outer target is increased by ~100% at the strike point and more than 500% at a position corresponding to 5 mm beyond the separtrix at the outer midplane (OMP). The magnetic connection length from the OMP to outer target is increased ~50% in the SFD. At the inner target, CD and SFD expansion and connection length are nearly identical. The divertor volume, indicated in Fig. 1, is increased from 0.04 m^3 in the CD to 0.11 m^3 in the SFD.

Single-null grids, desirable for their computational tractability, are used. In this discharge, the OMP separation of the primary separatrix and the secondary separatrix (connecting to the upper X-point) is 7 mm in the CD case and and 11 mm in the

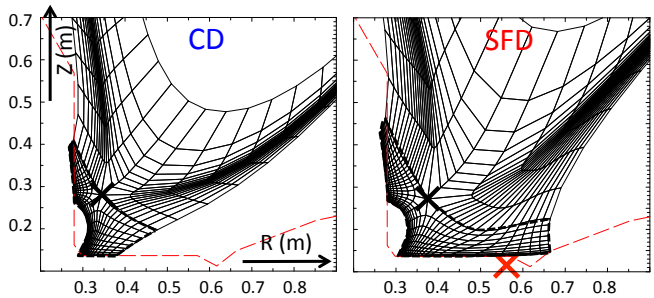

Figure 1: Divertor region of UEDGE grids for conventional divertor (CD) and snowflake divertor (SFD) simulations. Primary X-points are shown with black X's. The red X indicates the SFD secondary X-point. Divertor region control volumes used in the analysis are indicated with dashed lines.

SFD, limiting the grids to these relatively small OMP widths. As a result, the boundary conditions (BC) at the outer "walls" can significantly influence the UEDGE solutions.

In the analysis below, UEDGE is used in two modes. In "Mode 1," a range of separatrix shifts (δ_{sep}) and divertor target recycling (R_{div}) is explored to find the combination of these two key parameters that provides a fit to NSTX midplane and divertor diagnostic data. Specifically, Thomson scattering [14, 15] and charge exchange recombination spectroscopy [16] are matched at the OMP, and IR-thermography-based heat flux [17], and spectroscopic D_α emission [18] constrain the divertor solution. To facilitate Mode 1, radial diffusivity profiles are determined using the automated profile fitting procedure introduced by Canik [19]. All radial diffusivity profiles are assumed to be poloidally uniform. In "Mode 2," the density at the core-edge interface is varied, while holding other settings fixed, to compare CD and SFD physics. All solutions discussed in Section 3 are in steady state.

Power is input at the core boundary, split evenly between ion and electron channels. In Mode 1, ion input from the core matches the neutral beam injection. For 4-MW beam power, particle input is estimated to be 4.0×10^{20} s^{-1}. In Mode 2, the core density is fixed. At the outer wall, in Mode 1, density and temperatures are fixed as needed to match the OMP diagnostic data; in Mode 2, gradient scale length BC are employed for these quantities. In Mode 1, density is set to a single value along the wall, but the wall temperature profiles vary sinusoidally, from maxima at the OMP wall to 10 eV at a poloidal distance of 1.5 m from the OMP. (This reduction at locations far from the OMP prevents significant artificial inflow of energy to the divertor regions.) In both Modes, at the inner midplane, 1.9×10^{21} s^{-1} of neutral gas is injected, representing experimental injection at that location. At the private flux wall, the radial (i.e., perpendicular to flux surfaces) gradients of density and temperatures are set to 2 cm. Outer wall recycling (of both ions and neutrals) is 80 and 90% for the CD and SFD, respectively. (In the relatively narrow 7-mm CD grid, stronger pumping is needed to prevent excessive neutral density at the OMP.) At the private flux wall, ion recycling is again 80 and 90% for the CD and SFD, respectively, but neutral recycling is 100% for both configurations. For the targets, 100% neutral recycling is assumed in both Modes, and ion recycling is discussed in Section 3.

To improve modeling in the low-temperature PDD regime, the divertor target BC have been modified to include the transfer of power by neutral gas. Assuming a Maxwellian neutral distribution, gas power loss (GPL) is $q_{GPL} = 2\Gamma_g T_g$ [20], where Γ_g is the one-way flux and T_g is the neutral temperature (which is typically taken as equal to the ion temperature in the UEDGE combined ion-plus-neutral energy equation). Gas flux is assumed to recycle as molecules. The incident flux, Γ_g, is assumed to be purely atomic; in attached plasmas (and during detachment onset), just such an imbalance is expected — charge exchange strongly couples atomic neutrals to the main ion flow, driving them toward the target. To capture the energetics of molecules that dissociate and return to the target in atomic form, an additional boundary term, $\Gamma_g\varepsilon_{FC}$, is employed to transfer electron energy to the ion-plus-neutral fluid, modeling the Franck-Condon energy transfer associated with dissociation. (Note that this implementation ignores the molecular 4.5-eV bond energy itself, and radiative losses in the dissociation process.) In summary, the GPL fluxes to the target for ion-plus-neutral and electron fluids are, respectively, $q^{i+n}_{GPL} = 2\Gamma_g T_g - \Gamma_g\varepsilon_{FC}$, and $q^{e}_{GPL} = \Gamma_g\varepsilon_{FC}$.

3. Modeling results and discussion

As shown in Fig. 2, a scan of δ_{sep}-R_{div} parameter space shows a best-fit CD simulation at R_{div}=0.91 and δ_{sep}=2.1 cm. In this scan and the SFD scan discussed below, the δ_{sep} range from 1.7 to 2.2 cm corresponds to OMP electron separatrix temperatures (T_e^{sep}) from 52 to 82 eV. The scans use 3% fixed fraction. Fig. 2 also shows divertor profiles of heat flux and D_α emission for the best-fit simulation. The shortfall seen in the "tail" of the simulated heat flux could be related to the artificial outer wall boundary, which tends to extract power from the outer SOL. The low simulated D_α emission in the inner divertor region could be caused by the close proximity of the artificial private flux wall, or the lack of drift physics in the modeling. GPL terms have minimal impact in the CD, modifying peak heat flux and D_α emission results by <0.5% in the best-fit case.

In a similar SFD scan presented in Fig. 3, at δ_{sep}=1.8 cm and R_{div}=0.97, maximum outer divertor D_α emission reaches 500 ph/m^2/s, comparable to the experimentally measured emission. Without GPL terms described in Section 2, the heat flux in the δ_{sep}-R_{div} space is similar to that shown in Fig. 3, but D_α emission remains <100 ph/m^2/s. As shown in the radial profiles, simulated peak D_α emission and peak heat flux are similar to the experimental peaks, but the profile shapes differ. Diagreement could stem from a variety of factors, including those discussed above in relation to the CD D_α profile. Another consideration is that UEDGE neutral model limitations may be important in the cold, high-density SFD divertor.

The results shown in Figs. 2 and 3 suggest that R_{div} in the best-fit SFD is higher than in the CD (0.97 vs. 0.91). Though there is uncertainty due to modeling limitations, there are physical reasons to expect increased recycling in the detached SFD operation. At low target temperatures, low sheath voltage results in low-energy incident ions. These ions are more likely

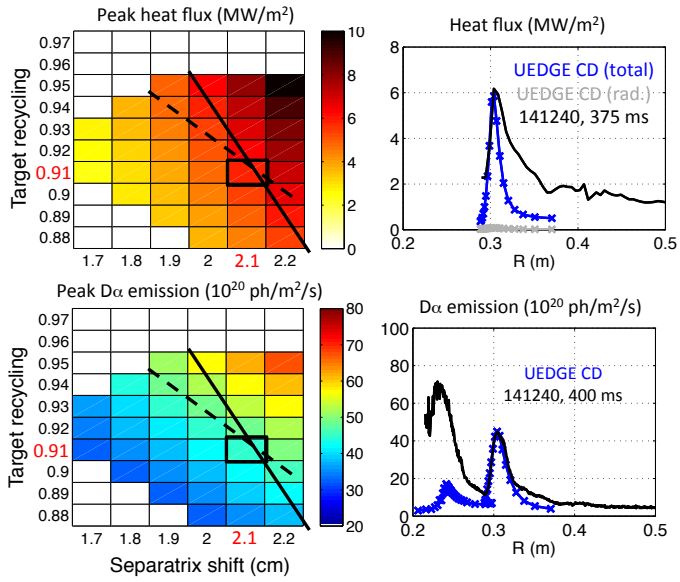

Figure 2: Conventional divertor δ_{sep}-R_{div} scan results. At left, maximum outer divertor heat flux and D_α emission are plotted in the δ_{sep}-R_{div} space. Approximate contours of the experimental data for heat flux and D_α emission are shown by the solid and dashed lines, respectively. For the simulation at the intersection of the two contours at R_{div}=0.91 and δ_{sep}=2.1 cm, heat flux and D_α emission profiles are shown at right.

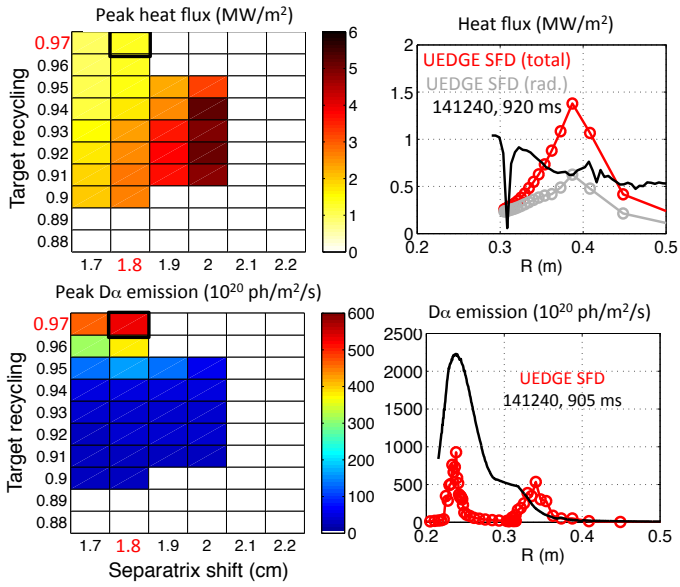

Figure 3: Snowflake divertor δ_{sep}-R_{div} scan results. At left, maximum outer divertor heat flux and D_α emission are plotted in the δ_{sep}-R_{div} space. For the simulation at R_{div}=0.97 and δ_{sep}=1.8 cm, heat flux and D_α emission profiles are shown at right.

to interact only in the upper layers of the target material, contributing to saturation of the deuterium retention mechanism. Also, the neutral particle flux in the SFD is 1-3×10^{24} $m^{-2}s^{-1}$ in the strike point region, compared to <10^{22} in the CD. (For reference, the peak ion fluxes in both SFD and CD cases are 1-2×10^{22} $m^{-2}s^{-1}$.) The chemistry of the NSTX lithium-conditioned graphite targets is complicated, but there is experimental evidence of saturation at NSTX-relevant deuterium ion fluences [21]; elevated neutral deuterium fluence and low-energy ion incidence in the SFD could accelerate such saturation.

Directly comparing the CD and SFD in a scan of core density (n_{core}) reveals the mechanisms by which SFD geometry enables partial detachment. 3% fixed fraction carbon is assumed, and target recycling is 95%. Uniform particle and thermal diffusivities, D=0.4 m^2/s, and $\chi_{i,e}$=10 m^2/s, similar to the values seen near the separatrix in the fitted solutions described above, are used. Results are summarized in Fig. 4. For both CD and SFD, panels (a)-(e) show evidence of partial detachment: several-hundred-fold increase in outer strike point (OSP) neutral gas denities, sub-eV OSP electron temperatures, reduced heat flux, increased radiation, and "rollover" in target particle flux. In the CD, detachment occurs gradually between n_{core}= 3 – 4 ×10^{19} m^{-3}, while in the SFD, detachment onset occurs sharply at n_{core}= 2.6 – 2.8 m^{-3}. The roles of three key features of SFD geometry can be identified: 1) Increased connection length (L_C). Fig. 4(c) shows similar $q_\parallel$ until SFD detachment onset, suggesting that perpendicular energy losses are not principally different in the SFD, despite increased L_C (which could enable such losses). Through 1D thermal conduction physics (cf. the two-point model [20]), increased L_C directly reduces T_e at the target. UEDGE naturally captures this effect, which is estimated to yield 20% lower T_e (given ~50% increase in L_C). 2) Increased divertor volume (V_{div}). With similar density, the increased SFD V_{div} results in a total divertor particle inventory of 2.1×10^{18} vs. 1.0×10^{18} in the CD. As seen in Fig. 4(d), the radiated power is correspondingly increased by a factor of two. 3) Increased wetted area (A_{wet}). Increased SFD A_{wet} accounts for the lower $q_\perp$ in Fig. 4(c) but, more importantly for detachment physics, enables GPL, which increases linearly with A_{wet}. GPL power extraction, shown in Fig. 4(d), contributes to $q_\parallel$ reduction, and acts as a trigger for strong recombination and associated partial detachment. GPL is pivotal in reducing T_e^{OSP} below 0.5 eV, inducing the jump in recombination shown in panel (e) — SFD simulations without GPL show T_e^{OSP} >0.5 eV and a modest rise in recombination to 0.3×10^{22} s^{-1} at n_{core}= 3.4 ×10^{19} m^{-3}. Thus, the modeling shows that the synergistic combination of these three features of SFD geometry reduce target T_e and $q_\parallel$, and promote partial detachment at much lower n_{core} than seen in the CD. Fig. 4(f) shows the total divertor plugging efficiency, ζ, defined as the ratio of ionization in the divertor volume to neutral sources, including recombination and recycling. For neutrals generated near the inner and outer strike points, the poloidal distances that must be traversed to escape the divertor region are similar in the CD and SFD. Similar ζ prior to attachment implies similar neutral transparency of the attached divertor plasmas. In detachment, ζ declines as cooler plasma conditions allow neutral leakage.

Modeling with charge-state-resolved carbon has been attempted. However, the carbon concentration in the divertor region is low (well below 3%), and does not yield enough radiation to enable detachment. The reasons for this must be unfolded in future research, but a prime culprit is the lack of plasma drift physics in the modeling. For example, estimating the OSP poloidal E×B drift velocity as $v_{ExB}^{pol.} = 3T_e/(\lambda_{Te}B_{tor.})$ [20],

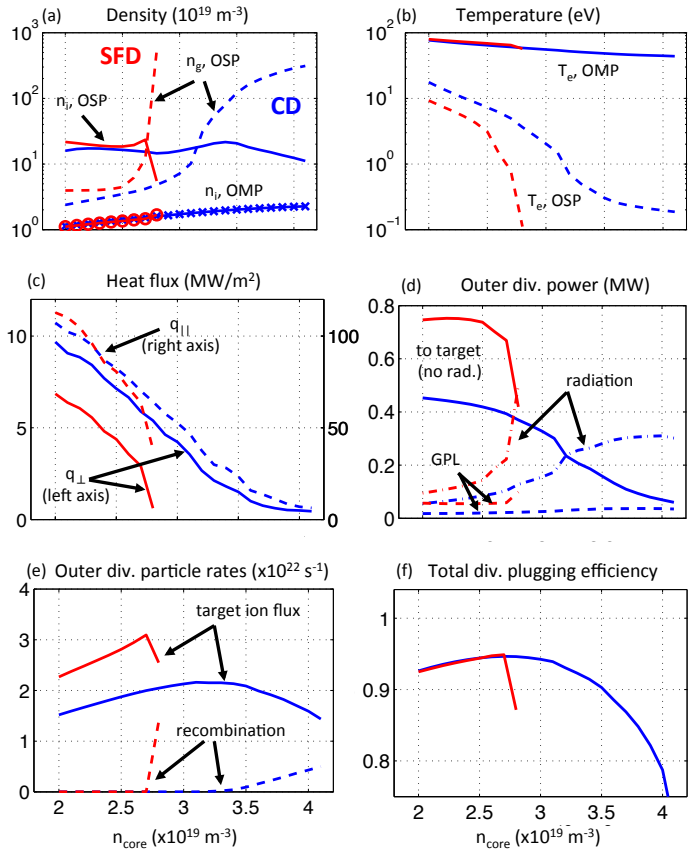

Figure 4: Results from scan of core density (n_{core}) for CD (blue) and SFD (red): (a) ion density at the outer midplane (OMP) separatrix, and ion and neutral gas density at the outer strike point (OSP); (b) electron temperatures at the OSP and OMP; (c) peak parallel and perpendicular incident heat fluxes; (d) total power incident on the outer divertor target, the gas power loss component of incident power, and the power radiated in the outer divertor volume; (e) ion flux to the outer target, and volumetric recombination; and (f) total divertor plugging efficiency.

and given $T_e \approx 20$ eV, $\lambda_{Te} \approx 0.05$ m, and B=1.2 T, gives $v_{ExB}^{pol.}$= 1000 m/s. This speed is comparable to the main ion poloidal flow speed for $T_{e,i} \approx 20$ eV at field line incidence ~2 degrees, which is 1500 m/s. Such strong drift flow could dramatically affect the carbon divertor compression effect which, in the absence of drifts, strongly concentrates carbon near the targets.

4. Conclusions

Results from UEDGE operated in a profile-fitting mode to recreate the edge and divertor plasma conditions in NSTX SFD experiments show a significantly higher target recycling in the SFD case: 97% in the vs. 91% in the CD. Higher R_{div} in the SFD could be related to partial saturation of the lithium-conditioned targets.

Using UEDGE in a mode with uniform diffusivities and R_{div}=0.95, core density is scanned to identify SFD physics effects. The dominant effect is the larger SFD V_{div}, which doubles divertor radiation, while increased A_{wet} and L_C play supporting roles in reducing target T_e and $q_{||}$, and inducing partial detachment. The GPL mechanism scales linearly with A_{wet} and triggers strong recombination and associated high neutral densities that might contribute to the target saturation and high recycling seen in the fitted SFD solution.

For conditioned targets, despite local saturation near the strike point(s), persistent strong pumping elsewhere might act to prevent full detachment, enabling the desired partial detachment. Spatially dependent recycling can be addressed in future experiments and modeling. In divertors without strongly pumping targets, SFD-induced saturation will obviously not be a distinguishing characteristic of the SFD.

SFD modeling might benefit from several extensions of the model used here. For example, including drifts might be especially important for charge-state resolved carbon modeling. Also, as underscored by the significant neutral gas effects identified in this work, more complete neutral modeling might be beneficial. Several aspects of the SFD concept are not addressed the present modeling, including instability-driven mixing in the region of weak poloidal field [6], and can be considered in future work.

5. Acknowledgments

This work has been performed under the auspices of the U.S. Department of Energy by Lawrence Livermore National Laboratory under Contract DE-AC52-07NA27344.

[1] A. Loarte, et al., Nucl. Fusion 47 (2007) S203.
[2] T. K. Gray, et al., J. Nucl. Mater. 415 (2011) S360 – S364.
[3] J. E. Menard, et al., Nucl. Fusion 52 (2012) 083015.
[4] J. E. Menard, et al., Nucl. Fusion 51 (2011) 103014.
[5] D. D. Ryutov, Phys. Plasmas 14 (2007) 064502.
[6] D. D. Ryutov, et al., Plasma Phys. Contr. Fusion 54 (2012) 124050.
[7] V. A. Soukhanovskii, et al., Nucl. Fusion 51 (2011) 012001.
[8] V. A. Soukhanovskii, et al., Phys. Plasmas 19 (2012) 082504.
[9] V. A. Soukhanovskii, et al., Phys. Plasmas 16 (2009) 022501.
[10] V. A. Soukhanovskii, et al., Nucl. Fusion 49 (2009) 095025.
[11] T. D. Rognlien, et al., J. Nucl. Mater. 196 (1992) 347 – 351.
[12] T. D. Rognlien, M. E. Rensink, Fusion Eng. Design 60 (2002) 497 – 514.
[13] S. I. Braginskii, Transport processes in a plasma, in: M. A. Leontovitch (Ed.), Rev. Plasma Phys., Vol. 1, Consultants Bureau, New York, NY, 1965, pp. 205 – 311.
[14] D. Johnson, et al., Rev. Sci. Instrum 70 (1) (1999) 776–779.
[15] B. P. LeBlanc, et al., Rev. Sci. Instrum 74 (3) (2003) 1659–1662.
[16] R. E. Bell, Rev. Sci. Instrum 77 (10).
[17] A. G. McLean, et al., Rev. Sci. Instrum. 83 (2012) 053706.
[18] V. A. Soukhanovskii, et al., Rev. Sci. Instrum 74 (3) (2003) 2094–2097.
[19] J. M. Canik, et al., J. Nucl. Mater. 415 (2011) S409 – S412.
[20] P. C. Stangeby, The plasma boundary of magnetic fusion devices, IOP publishing Ltd., 2000.
[21] C. N. Taylor, et al., J. Nucl. Mater. 415 (2011) S777 – S780.
[22] C. N. Taylor, Fundamental mechanisms of deuterium retention in lithiated graphite plasma facing surfaces, Ph.D. thesis, Purdue University (2012).